Quantum-Statistical Distribution Functions of a Hard-Sphere System*†

C. J. NISTERUK‡ AND A. ISIHARA
Department of Physics, State University of New York, Buffalo, New York
(Received 1 August 1966)

The singlet and pair distribution functions of a hard-sphere fluid are evaluated. Diagrams in various orders in the hard-sphere diameter a are analyzed. The pseudopotential and the binary-kernel methods are compared. At low temperatures the contribution from chain diagrams is evaluated explicitly in terms of the modified Bessel and Struve functions. These chain diagrams are important at large distances or at low energy. At short distances, first-order diagrams have to be examined, and classical and quantum-mechanical cases are treated.

I. INTRODUCTION

THE similarity of a hard-sphere Bose gas to liquid He^4 at lowest temperatures has made it the object of intensive study for nearly a decade. Apart from this, however, the quantum statistical many-body theory of a hard-sphere gas is of interest in its own right because of the wide range of problems characterized by very strong repulsive interactions.

The aim of this paper is to investigate the spatial correlation of a hard-sphere gas by evaluating the singlet and pair-distribution functions. For this purpose an extension of the recent work by Yee and Isihara[1] will be made. These authors evaluated the pair-distribution function (p.d.f. hereafter) of a hard-sphere Bose gas by the binary-kernel method. Following Lee and Yang[2] they avoided the complications arising from condensation by considering the gas at the lowest temperature obeying Boltzmann statistics, and discussed two types of diagrams, namely, the chain and tick-tack-toe.

In this paper we approach the problem from a more general point of view in the following sense: First, we compare the binary kernel method with the approach previously developed by Fujita, Isihara, and Montroll[3] for Fourier transformable potentials. Second, we introduce a more general set of chain diagrams to be called hybrid and examine the role of the simple chain and tick-tack-toe diagrams as special cases. Third, we evaluate not only the p.d.f. but also the singlet-distribution function. Fourth, we investigate the hard-sphere gas at a finite temperature. For this purpose, in the Boltzmann case, we evaluate the eigenvalues of a certain integral equation; these are used to arrive at a low-temperature expression for the p.d.f. For the Bose gas, we consider the exchange of particles characteristic of Bose statistics and show that the results reported by Colin and Peretti[4] require some correction.

Summarizing, in this paper we attempt to generalize the treatment of Ref. 1 and present various new results which improve upon those previously reported. In addition, we examine the short-distance behavior of the p.d.f. in view of the recent criticism of Lee, Huang, and Yang's[5] work by Luban.[6]

II. THE PSEUDOPOTENTIAL AND BINARY-KERNEL METHODS

To gain an understanding of the strange behavior of liquid helium, Lee and Yang and many other investigators made attempts at evaluation of the ground-state and excited-state energies of a hard-sphere gas. Theoretically it is essential here to find suitable methods of treating the hard-sphere potential. It was Lee, Huang, and Yang[5,7,8] who developed the pseudopotential and the binary-kernel methods.

In the S-wave approximation the pseudopotential is given by

$$\phi=8\pi a\delta(\mathbf{r}_1-\mathbf{r}_2)(\partial/\partial r_{12})r_{12}\,, \tag{2.1}$$

where a is the hard-sphere diameter. The differential operator $(\partial/\partial r)r$ in this expression is important but Lee and Yang showed that with a certain amount of caution one could use the next approximate expression:

$$\phi'=8\pi a\delta(\mathbf{r}_1-\mathbf{r}_2)\,. \tag{2.2}$$

This approximate expression is very convenient because the δ function allows one to take the Fourier transform of the potential.

The binary kernel $B(\beta)$ is derived from the two-particle cluster operator:

$$U_2=e^{-\beta H_2}-e^{-\beta H_2^0}\,, \tag{2.3}$$

where H_2 is the two particle Hamiltonian, H_2^0 is that for free particles, and $\beta=1/kT$. The binary kernel is then defined by

$$B=(\partial U_2/\partial\beta)+H_2^0U_2\,. \tag{2.4}$$

* This work was supported by the National Science Foundation.
† Taken from the dissertation submitted by one of the authors (C. J. Nisteruk) to the faculty of the Polytechnic Institute of Brooklyn in partial fulfillment of the requirements for the degree of Doctor of Philosophy, 1966.
‡ Present address: Manhattan College, New York, New York.
[1] A. Isihara and D. D. H. Yee, Phys. Rev. **136**, A618 (1966); Physica **30**, 2123 (1966).
[2] T. D. Lee and C. N. Yang, Phys. Rev. **116**, 25 (1959); **117**, 12 (1960).
[3] S. Fujita, A. Isihara, and E. W. Montroll, Bull. Classe Sci. Acad. Roy. Belg. **44**, 1018 (1958).
[4] L. Colin and J. Peretti, J. Math. Phys. **1**, 97 (1960).
[5] T. D. Lee, K. Huang, and C. N. Yang, Phys. Rev. **106**, 1135 (1957), hereafter referred to as LHY.
[6] M. Luban, Phys. Rev. **138**, A1033 (1965).
[7] K. Huang and C. N. Yang, Phys. Rev. **105**, 767 (1957).
[8] T. D. Lee and C. N. Yang, Phys. Rev. **105**, 1119 (1957); **113**, 1165 (1959).

The advantage of introducing B is in its explicit dependence on U_2 rather than on the potential function. Thus its matrix elements exist even for the case of hard spheres.

The hard-sphere binary kernel is rather complicated, but for small a Lee and Yang showed that one can approximate B as follows:

$$B=B_1+B_2+\cdots,$$

$$\langle \mathbf{k}_1',\mathbf{k}_2'|B_1|\mathbf{k}_1,\mathbf{k}_2\rangle = -(a/\pi^2)\delta(\mathbf{k}_1'+\mathbf{k}_2'-\mathbf{k}_1-\mathbf{k}_2)e^{-\beta(k_1^2+k_2^2)},$$

$$\langle \mathbf{k}_1',\mathbf{k}_2'|B_2|\mathbf{k}_1,\mathbf{k}_2\rangle = (a^2/\pi^{5/2})\delta(\mathbf{k}_1'+\mathbf{k}_2'-\mathbf{k}_1-\mathbf{k}_2)e^{-\beta(k_1^2+k_2^2)} \times\left[2k\int_0^{(2\beta)^{1/2}k}\exp t^2dt-(2\beta)^{-1/2}\exp(2\beta k^2)\right], \quad (2.5)$$

where

$$k=\tfrac{1}{2}|\mathbf{k}_1-\mathbf{k}_2|. \quad (2.6)$$

We shall now show that to first order in a use of the approximate pseudopotential of Eq. (2.2) is equivalent to the binary-kernel method in the evaluation of the p.d.f. For this purpose, one may consider the coordinate-space representation of B_1 acting over the reciprocal temperature interval $(\beta'-\beta'')$:

$$B_1=-\phi_{12}'e^{(\beta'-\beta'')(\nabla_1^2+\nabla_2^2)}. \quad (2.7)$$

It turns out that ϕ_{12}' here is precisely the approximate pseudopotential of Eq. (2.2). Thus B_1 is equivalent to free propagation of two particles over the interval $(\beta'-\beta'')$ terminated by an isothermal interaction corresponding to ϕ_{12}'. Alternately, in momentum space the two particle propagator of Fig. 1(b) is

$$K(\mathbf{k}_a,\mathbf{k}_b,\beta';\mathbf{k}_1,\mathbf{k}_2,\beta'')=\int\delta(\mathbf{k}_a-\mathbf{k}_1+\mathbf{q})e^{-(\beta'-\beta'')k_1^2} \times[-v(q)]\delta(\mathbf{k}_b-\mathbf{k}_2-\mathbf{q})e^{-(\beta'-\beta'')k_2^2}d\mathbf{q}, \quad (2.8)$$

where $v(q)$ is the Fourier transform of the potential ϕ_{12}:

$$v(q)=\frac{1}{(2\pi)^3}\int\phi_{12}e^{-i\mathbf{q}\cdot\mathbf{r}}d\mathbf{r}. \quad (2.9)$$

For $\phi'(r)$ of Eq. (2.2) we have

$$v(q)=a/\pi^2. \quad (2.10)$$

Thus we find

$$K(\mathbf{k}_a,\mathbf{k}_b,\beta';\mathbf{k}_1,\mathbf{k}_2\beta'')=-(a/\pi^2)\delta(\mathbf{k}_a+\mathbf{k}_b-\mathbf{k}_1-\mathbf{k}_2) \times\exp[-(\beta'-\beta'')(k_1^2+k_2^2)]. \quad (2.11)$$

This is simply the first-order binary kernel. Hence, the diagrammatic equivalence in Fig. 1.

We can then proceed to consider chain diagrams such as shown in Fig. 2. According to Fujita, Isihara, and

FIG. 1. Diagrams for the binary kernel and pseudopotential.

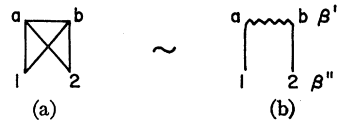

Montroll the p.d.f. corresponding to such a chain is

$$\rho^{(2)}(r)-\rho^2=\sum_{l\geq 2}\frac{z^l}{\beta h^6}\sum_t\int[-v(q)]^{l-1} \times\Lambda^l(q,t)e^{(i/\hbar)\mathbf{q}\cdot\mathbf{r}}d\mathbf{q}, \quad (2.12)$$

where ρ is the number density, z the absolute activity, and Λ, the eigenvalues, are

$$\Lambda(q,t)=\left(\frac{2\pi m}{\beta}\right)^{3/2}\int_0^\beta e^{-(q^2/2m\beta)\alpha(\beta-\alpha)}e^{-i2\pi t(\alpha/\beta)}d\alpha. \quad (2.13)$$

We adopt units such that $2m=\hbar=1$ and change the variable of integration from q to $2q$ to correspond with Eq. (3.1) in the next section. Then with

$$\lambda_t(q,\lambda)\equiv(\beta^{1/2}/\pi^{3/2})\Lambda(2q,t)=\int_0^1 e^{-4\beta q^2x(1-x)}e^{-i2\pi tx}dx, \quad (2.14)$$

and $v(q)$ of Eq. (2.10), we have

$$\rho^{(2)}(r)-\rho^2=-\frac{32\pi^3}{a\lambda^2}\sum_{l\geq 2}\sum_t\frac{1}{(2\pi)^6}\int\left(-\frac{2az}{\lambda}\lambda_t\right)^l \times e^{2i\mathbf{q}\cdot\mathbf{r}}d\mathbf{q}, \quad (2.15)$$

where λ is the de Broglie thermal wavelength.

Equation (2.15) is exactly that obtained in Ref. 1 by the binary-kernel method. We have therefore shown the equivalence of the two methods insofar as the first-order pseudopotential and binary kernel are concerned.

The ground-state energy of a hard-sphere system may be expressed in terms of the pair distribution function. As Fujita and Hirota[9] showed, one has

$$E=E_{\text{ideal}}(0)+\tfrac{1}{2}V\int_0^1 d\kappa\int d\mathbf{r}\,\phi(r)\rho^{(2)}(r;\kappa a), \quad (2.16)$$

where κ represents a coupling parameter and $\rho^{(2)}(r;\kappa a)$ is obtained from $\rho^{(2)}(r;a)$ by replacing a by κa. If one then uses the pseudopotential and assumes $E_{\text{ideal}}(0)=0$, one obtains

$$E=4\pi\rho aN-\tfrac{1}{2}\textstyle\sum_k\{k_0^2+k^2-k(k^2+2k_0^2)^{1/2}\} \quad (2.17)$$

where

$$k_0^2=8\pi a\rho. \quad (2.18)$$

Equation (2.17) is exactly what Lee and Yang obtained. The divergent term is to be subtracted as

FIG. 2. Chain diagram.

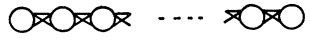

[9] S. Fujita and R. Hirota, Phys. Rev. 118, 6 (1960).

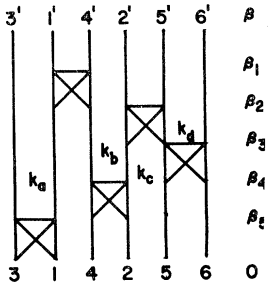

FIG. 3. Hybrid-chain diagram.

Lee and Yang pointed out. It is due to the approximation in the pseudopotential.

III. HYBRID DIAGRAMS

As mentioned in the previous section, Eq. (2.15) can be obtained by the binary-kernel method. In this section we use this method to evaluate the p.d.f. from a more general point of view than before. We start with the general formula[1] for the p.d.f.

$$\rho^{(2)}(r)=[\rho^{(1)}]^2+\frac{1}{(2\pi)^6}\int N(q)e^{2i\mathbf{q}\cdot\mathbf{r}}d\mathbf{q}, \tag{3.1}$$

where $N(q)$ is related to the Uhlenbeck functions as follows:

$$N(q)=\sum_{l=2}^{\infty}\frac{z^l}{(l-2)!}u_l(q); \tag{3.2}$$

$$\int\langle\mathbf{r}^l|\,U_l\,|\mathbf{r}^l\rangle d\mathbf{r}^{l-2}=\frac{1}{(2\pi)^6}\int u_l(q)e^{2i\mathbf{q}\cdot(\mathbf{r}_2-\mathbf{r}_1)}d\mathbf{q}. \tag{3.3}$$

Let us use these formulas for diagrams such as shown in Fig. 3. Here, the two particles 1 and 2 have a linear chain of binary interactions inside and outside. For simplicity's sake we may first write the integral associated with the particular diagram of Fig. 3 and then consider a more general case.

We have

$$\begin{aligned}\langle\mathbf{k}'^6|\,U_6\,|\mathbf{k}^6\rangle=&\int_0^{\beta}d\beta_1\int_0^{\beta_1}d\beta_2\int_0^{\beta_2}d\beta_3\int_0^{\beta_3}d\beta_4\int_0^{\beta_4}d\beta_5\int\cdots\int d\mathbf{k}_a d\mathbf{k}_b d\mathbf{k}_c d\mathbf{k}_d\,\exp\{-(\beta-\beta_5)k_3'^2-(\beta-\beta_1)(k_1'^2+k_4'^2)\\&-(\beta-\beta_2)(k_2'^2+k_5'^2)-(\beta-\beta_3)k_6'^2\}\langle\mathbf{k}_1',\mathbf{k}_4'|\,B(\beta_1-\beta_2)\,|\mathbf{k}_a,\mathbf{k}_b\rangle\exp\{-(\beta_2-\beta_5)k_a^2\}\langle\mathbf{k}_3',\mathbf{k}_a|\,B(\beta_5)\,|\mathbf{k}_3,\mathbf{k}_1\rangle\\&\times\exp\{-(\beta_2-\beta_4)k_b^2\}\langle\mathbf{k}_2',\mathbf{k}_5'|\,B(\beta_2-\beta_3)\,|\mathbf{k}_c,\mathbf{k}_d\rangle\exp\{-(\beta_3-\beta_4)k_c^2\}\langle\mathbf{k}_b,\mathbf{k}_c|\,B(\beta_4-\beta_5)\,|\mathbf{k}_4,\mathbf{k}_2\rangle\\&\times\exp\{-\beta_5(k_4^2+k_2^2)\}\langle\mathbf{k}_d,\mathbf{k}_6'|\,B(\beta_3-\beta_4)\,|\mathbf{k}_5,\mathbf{k}_6\rangle\exp\{-\beta_4(k_5^2+k_6^2)\}.\end{aligned} \tag{3.4}$$

Substituting the first-order binary kernel B_1, integrating over $\mathbf{k}_a$, $\cdots$, $\mathbf{k}_d$, and setting $\mathbf{k}_i'=\mathbf{k}_i$ for $i\geqq 3$ we obtain

$$\begin{aligned}&u_6(\mathbf{k}_1',\mathbf{k}_2';\mathbf{k}_1,\mathbf{k}_2)\\&=\left(-\frac{a}{\pi^2}\right)^5\int_0^{\beta}\cdots\int_0^{\beta_4}d\beta_5\int d\mathbf{k}_3 d\mathbf{k}_4 d\mathbf{k}_5 d\mathbf{k}_6\\&\quad\times\exp\{-\beta(k_3^2+k_5^2+k_6^2)-\beta(k_1'^2+k_2'^2)\\&\quad+\beta_1(k_1'^2-k_1^2)+\beta_4(k_2'^2-k_2^2)-(\beta-\beta_1)k_4^2\\&\quad-(\beta-\beta_1)(\mathbf{k}_4+\mathbf{k}_1'-\mathbf{k}_1)^2-\beta_4k_4^2\}.\end{aligned} \tag{3.5}$$

We introduce the relative and center-of-mass momenta

$$\begin{aligned}&\mathbf{k}=\tfrac{1}{2}(\mathbf{k}_1-\mathbf{k}_2);\quad &&\mathbf{k}'=\tfrac{1}{2}(\mathbf{k}_1'-\mathbf{k}_2')\\&\mathbf{K}=\mathbf{k}_1+\mathbf{k}_2;\quad &&\mathbf{K}'=\mathbf{k}_1'+\mathbf{k}_2'\\&\mathbf{Q}=\mathbf{k}+\mathbf{k}';\quad &&\mathbf{q}=\tfrac{1}{2}(\mathbf{k}-\mathbf{k}')\end{aligned} \tag{3.6}$$

and integrate u_6 over $\mathbf{K}$, $\mathbf{K}'$, and $\mathbf{Q}$ to obtain

$$\begin{aligned}u_6(q)=&\left(-\frac{a}{\pi^2}\right)^5\left(\frac{\pi}{\beta}\right)^6\left(\frac{2\pi}{\beta}\right)^3\beta^5\int_0^1 dx_1\int_0^{x_1}dx_2\cdots\int_0^{x_4}dx_5\\&\times G(\sigma;1-x_4)G(\sigma;|x_4-x_1|)G(\sigma;x_1),\end{aligned} \tag{3.7}$$

where

$$\begin{aligned}&G(\sigma;|x_i-x_j|)=\exp[-\sigma|x_i-x_j|\{1-|x_i-x_j|\}];\\&\sigma=4\beta q^2.\end{aligned} \tag{3.8}$$

The integral in $u_6(q)$ is still time-ordered. However, there are 5! similar diagrams which differ only in time ordering. These arise from the vertical permutations of the binary kernel. Their sum may effectively be expressed by extending the limits of integration.

In general, we consider a chain which consists of l particles such that $s-2$ particles are between 1 and 2 and t particles outside:

$$l=s+t. \tag{3.9}$$

The consideration of the above special case gives the following rules:

(1) To each binary kernel corresponds a factor $(-a/\pi^2)$;

(2) integration over each of the t outside particles gives a factor $(\pi/\beta)^{3/2}$;

(3) integration over each of the $s-2$ momenta between the particles 1 and 2 gives a factor $(\pi/\beta)^{3/2}$;

(4) integrations on the center of mass momenta $\mathbf{K}$ and $\mathbf{Q}$ give a factor $(2\pi/\beta)^3$;

(5) there are $(l-1)!$ similar diagrams arising from permutations of the binary crosses;

(6) the total number of β_k integrations is $l-1$. The transformation from $d\beta_k$ to dx_k introduces a factor β^{l-1};
(7) the number of combinations of choosing $s-2$ particles out of $l-2$ particles is ${}_{(l-2)}C_{(s-2)}$. To each of these combinations there correspond different diagrams resulting from the permutations $(s-2)!$ and $t!$ of the particles "inside" and "outside" 1 and 2. A factor $(l-2)!$ is the result.

Considering all these factors, we have for the general case

$$u_{s,l-s}(q)=\left(-\frac{a}{\pi^2}\right)^{l-1}\left(\frac{\pi}{\beta}\right)^{3/2(l-2)}\left(\frac{2\pi}{\beta}\right)^{3}(l-2)!$$
$$\times\beta^{l-1}\int_0^1 dx_1\int_0^1 dx_2\cdots\int_0^1 dx_{s-1}G(1-x_1)$$
$$\times G(|x_1-x_2|)\cdots G(|x_{s-2}-x_{s-1}|)$$
$$\times G(x_{s-1}). \quad (3.10)$$

It is then appropriate to introduce the integral equation

$$\lambda_n\psi_n(x)=\int_0^1 G(\sigma;|x-y|)\psi_n(y)dy. \quad (3.11)$$

One may consider G to be periodic in the domain (0,1) and take

$$\psi_n(x)=e^{2\pi inx}. \quad (3.12)$$

Then, we arrive at

$$u_{s,l-s}(q)=-\frac{32\pi^3}{a\lambda^2}\left(-\frac{2a}{\lambda}\right)^{l}(l-2)!\sum_{m=-\infty}^{\infty}\lambda_m{}^{s}. \quad (3.13)$$

To obtain $u_l(q)$ appearing in Eq. (3.2) it is necessary to sum over all diagrams corresponding to the various partitions of $l=s+t$. Thus

$$u_l(q)=\sum_{s=2}^{l}u_{s,l-s}$$
$$=-\frac{32\pi^3}{a\lambda^2}\left(-\frac{2a}{\lambda}\right)^{l}(l-2)!\sum_{s=2}^{l}\sum_{m=-\infty}^{\infty}\lambda_m{}^{s}, \quad (3.14)$$

where λ is the de Broglie thermal wavelength

$$\lambda=(4\pi\beta)^{1/2}. \quad (3.15)$$

The simple-chain result (particles 1 and 2 terminal) can be obtained from Eq. (3.14) if we set $s=l$. The tick-tack-toe result corresponds to the cases $s=2$, $l\geq 3$. Therefore, we call the diagrams of the type of Fig. 3 hybrid and, correspondingly, express $N(q)$ defined by Eq. (3.2) as follows:

$$N_H(q)=-64\pi^3\frac{z}{\lambda^3}\sum_{l=0}^{\infty}\left(-\frac{2az}{\lambda}\right)^{l}$$
$$\times\sum_m\left(\lambda_m-\frac{\lambda_m}{1+(2az/\lambda)\lambda_m}\right). \quad (3.16)$$

At this stage we note that the singlet-distribution function corresponding to the Boltzmann chain approximation is given by

$$\rho^{(1)}=\frac{1}{(2\pi)^3}\sum_{l=1}^{\infty}\frac{z^l}{(l-1)!}\int\langle\mathbf{k}^l|u_l|\mathbf{k}^l\rangle d\mathbf{k}^l$$
$$=\frac{z}{\lambda^3}\sum_{l=0}^{\infty}\left(-\frac{2az}{\lambda}\right)^{l}. \quad (3.17)$$

Therefore, Eq. (3.16) may be rewritten as follows:

$$N_H(q)=-64\pi^3\rho^{(1)}\sum_m\left(\lambda_m-\frac{\lambda_m}{1+(2az/\lambda)\lambda_m}\right). \quad (3.18)$$

Note here that the contribution from tick-tack-toe diagrams does not appear except through $\rho^{(1)}$. Therefore, if we replace $\rho^{(1)}$ by ρ, we shall be able to obtain only the chain-diagram results.

The eigenvalues λ_m may be evaluated easily. We find at very low temperatures the following asymptotic expression:

$$\lambda_m=\Lambda_m+\Lambda_m{}^1;$$
$$\Lambda_m=\frac{2\sigma}{\sigma^2+\omega^2};\quad \Lambda_m{}^1=4\sigma^2\frac{\sigma^2-3\omega^2}{(\sigma^2+\omega^2)^3}, \quad (3.19)$$

where

$$\omega=2\pi m. \quad (3.20)$$

The contribution to the p.d.f. from $N_H(q)$ of Eq. (3.18) starts with the two-particle U_2 function as can be seen from Eq. (3.2). Since U_2 is most important at short distances it may be appropriate to examine its contribution separately.

If U_2 is "expanded" in the first-order binary kernel and the resulting integral contracted in terms of $\lambda_m=\Lambda_m$, one obtains $-2a\rho^2/r$ for $\rho^{(2)}-\rho^2$. An attempt to extend the result to finite temperatures using Eq. (3.19) leads to a divergent integral. However, one may circumvent this difficulty by appeal to the exact quantum mechanical expression for the diagonal matrix elements of U_2 or by evaluating the integral alluded to without recourse to the eigenvalue technique. The latter procedure is straightforward for the two-particle case. One finds

$$\langle\mathbf{r}_1,\mathbf{r}_2|U_2|\mathbf{r}_1,\mathbf{r}_2\rangle=-\frac{2a}{r}\frac{1}{\lambda^6}e^{-r^2/2\beta}. \quad (3.21)$$

The exact expression is

$$\langle\mathbf{r}_1,\mathbf{r}_2|U_2|\mathbf{r}_1,\mathbf{r}_2\rangle$$
$$=\frac{1}{2\pi\lambda^4r^2}\begin{cases}e^{-r^2/2\beta}-e^{-(r-a)^2/2\beta}; & (r>a)\\ e^{-r^2/2\beta}-1; & (r<a)\end{cases} \quad (3.22)$$

Comparison of Eq. (3.22) taken to first order in a with Eq. (3.21) obtained from the first-order binary kernel

shows agreement for $r>a$. For $r<a$, B_1 fails to reproduce U_2 correctly.

In the low density limit ($z\to\rho\lambda^3$) and for small $r>a$ we thus obtain to first order in a

$$D(r)\equiv\rho^{-2}\rho^{(2)}(r)=1+\lambda^6\langle\mathbf{r}_1,\mathbf{r}_2|\,U_2\,|\,\mathbf{r}_1,\mathbf{r}_2\rangle+\cdots$$
$$=1-(2a/r)e^{-2\pi r^2/\lambda^2}+\cdots. \quad (3.23)$$

To evaluate the correlation function $D(r)$ to the second order in a it is necessary to augment Eq. (3.21) including terms of $O(a^2)$ and to consider the three-particle diagrams with first-order binary-kernel interactions. Unfortunately, the latter contribution to $\rho^{(2)}(r)$ diverges even for $\lambda_m=\Lambda_m$. The failure of $\Lambda_m{}^1$ to yield a finite contribution to $\rho^{(2)}(r)$ for the two-particle case is on a par with the failure of Λ_m at $T=0$ to give individually convergent results for $l\geq 3$. However, as shown in Ref. 1, the sum over Λ_m in Eq. (3.18) gives a finite reasonable result. Thus, we shall use a perturbation method in evaluating the sum of Eq. (3.18).

We write

$$f(\lambda_m)=\lambda_m-\frac{\lambda_m}{1+(2az/\lambda)\lambda_m}$$
$$=f_m{}^0+f_m{}^1, \quad (3.24)$$

where

$$f_m{}^0=f(\Lambda_m)$$
$$f_m{}^1=\{1-[1+(2az/\lambda)\Lambda_m]^{-2}\}\Lambda_m{}^1. \quad (3.25)$$

Then

$$\sum_m f_m{}^0=\frac{2}{\sigma}\sum_m\left\{\frac{1}{1+\xi_m{}^2}-\frac{1}{1+\xi_m{}^2+(2az/\lambda)(2/\sigma)}\right\}, \quad (3.26)$$

where

$$\xi_m=\omega/\sigma. \quad (3.27)$$

At low temperatures we may replace the summation by integration:

$$\sum_m\to\frac{\sigma}{2\pi}\int_{-\infty}^{\infty}d\xi. \quad (3.28)$$

Thus, Eq. (3.26) becomes

$$\sum_m f_m{}^0=\frac{1}{\pi}\int_{-\infty}^{\infty}\left(\frac{1}{1+\xi^2}-\frac{1}{1+\xi^2+\gamma/q^2}\right)d\xi$$
$$=1-[1+(\gamma/q^2)]^{-1/2}, \quad (3.29)$$

where

$$\gamma=4\pi az/\lambda^3. \quad (3.30)$$

Similarly

$$\sum_m f_m{}^1=\frac{2}{\pi\sigma}\int\left\{\frac{4}{(1+\xi^2)^3}-\frac{3}{(1+\xi^2)^2}\right\}$$
$$\times\left\{1-\frac{(1+\xi^2)^2}{(1+\xi^2+\gamma/q^2)^2}\right\}d\xi. \quad (3.31)$$

Upon integration we find

$$\sum_m f_m{}^1=\frac{8\pi}{\lambda^2}\left\{\frac{1}{2\gamma}\frac{q^3}{(q^2+\gamma)^{3/2}}\right.$$
$$\left.-\frac{q^2}{\gamma^2}\left(1-\frac{q}{(q^2+\gamma)^{1/2}}\right)+\frac{3}{8}\frac{q}{(q^2+\gamma)^{3/2}}\right\}. \quad (3.32)$$

The right-hand side contains terms which do not decrease with q. However such terms cancel with each other and the right-hand side decreases as a whole as q^{-2}. Thus, its Fourier transformation is possible.

In the low-density approximation we may use

$$z\to\rho\lambda^3,\quad \gamma\to\gamma_0=4\pi a\rho;\quad N_H(q)\to N_c(q).$$

Corresponding to the split of λ_m in Eq. (3.19), we write

$$N_c(q)=N_c{}^0(q)+N_c{}^1(q)$$
$$=-64\pi^3\rho[\textstyle\sum_m f_m{}^0+\sum_m f_m{}^1]. \quad (3.33)$$

Correspondingly, we have

$$D(r)=D^0(r)+D^1(r). \quad (3.34)$$

The function $D^0(r)$ represents the correlation function at the lowest temperature. $D^1(r)$ is its correction at a finite temperature. Both functions are evaluated for Boltzmann statistics. We shall later consider the exchange effects due to Bose statistics. The evaluation of $D^0(r)$ or $D^1(r)$ is now straightforward. We shall discuss these separately in the following sections.

IV. THE CORRELATION FUNCTION $D^0(r)$

In the previous section we noted the importance of the two-particle cluster function in the short-range behavior of the p.d.f. It was further observed that B_1 fails to reproduce it within the hard-sphere boundary. We therefore treat its contribution to the p.d.f. separately and delete it from $N_c{}^0(q)$ by summing on chains starting with $l=3$

$$N_c{}^1(q)=-\frac{32\pi^3}{a\lambda^2}\sum_{l=3}^{\infty}\sum_m\left(-\frac{2az}{\lambda}\lambda_m\right)^l$$
$$=-64\pi^3\rho\left\{1-\left(1+\frac{\gamma_0}{q^2}\right)^{-1/2}-\frac{\gamma_0}{2q^2}\right\}. \quad (4.1)$$

Consequently, we arrive at

$$D^0(r)=1+\lambda^6\langle\mathbf{r}_1,\mathbf{r}_2|\,U_2\,|\,\mathbf{r}_1,\mathbf{r}_2\rangle$$
$$-\frac{1}{\rho\pi^3}\int\left\{1-\left(1+\frac{\gamma_0}{q^2}\right)^{-1/2}-\frac{\gamma_0}{2q^2}\right\}e^{2i\mathbf{q}\cdot\mathbf{r}}d\mathbf{q}. \quad (4.2)$$

Using this expression and the exact Eq. (3.22) taken in the low T limit,

$$\langle\mathbf{r}_1,\mathbf{r}_2|\,U_2\,|\,\mathbf{r}_1,\mathbf{r}_2\rangle=\frac{1}{\lambda^6}\begin{cases}-2a/r+a^2/r^2; & (r>a)\\ -1; & (r<a)\end{cases} \quad (4.3)$$

we evaluate $D^0(r)$ as follows:

1. Exterior of Hard Sphere

For $r>a$, the first-order form of U_2 cancels the contribution $2a/r$ from the term $\gamma_0/2q^2$. As a result, we obtain

$$D^0(r)-1=-\frac{2\gamma_0}{\pi^2\rho r}\int_0^\infty\left\{1-\frac{\eta}{(1+\eta^2)^{1/2}}\right\}\eta\sin\eta\zeta d\eta, \quad (4.4)$$

where

$$\begin{aligned}\gamma_0&=4\pi a\rho,\\ \eta&=\gamma_0^{-1/2}q,\\ \zeta&=r/r_c,\\ r_c^{-1}&=2\gamma_0^{1/2}=(16\pi a\rho)^{1/2}.\end{aligned} \quad (4.5)$$

The integral of Eq. (4.4) is evaluated in Appendix A. We arrive at

$$\begin{aligned}D^0(r)-1&=-(4a/r)\zeta\Phi(\zeta)\\ &=-16\pi^{1/2}(a^3\rho)^{1/2}\Phi(\zeta).\end{aligned} \quad (4.6)$$

Here $\Phi(\zeta)$ is defined by

$$\zeta\Phi(\zeta)=G_0(\zeta)-(1/\zeta)G_1(\zeta). \quad (4.7)$$

The function G_ν is the difference of the modified Bessel and Struve functions:

$$\begin{aligned}G_\nu(\zeta)&\equiv I_\nu(\zeta)-L_\nu(\zeta),\\ &=\sum_{j=0}^\infty\frac{(-)^j(\frac{1}{2}\zeta)^{j+\nu}}{\Gamma[(j/2)+1]\Gamma[(j/2)+\nu+1]}.\end{aligned} \quad (4.8)$$

Thus,

$$\zeta\Phi(\zeta)=\tfrac{1}{4}\sum_{j=0}^\infty(-)^j\frac{(j+1)(j+2)}{[\Gamma(\frac{1}{2}j+2)]^2}\left(\frac{\zeta}{2}\right)^j. \quad (4.9)$$

In particular, at large distances

$$\begin{aligned}\Phi(\zeta)&\sim\frac{1}{\pi^2}\sum_{k=0}^\infty 2^{(2k+1)}(2k+1)(2k+2)\Gamma^2(k+\tfrac{1}{2})\zeta^{-(2k+4)}\\ &\sim\frac{4}{\pi\zeta^4}=\frac{4}{\pi}\left(\frac{r_c}{r}\right)^4.\end{aligned} \quad (4.10)$$

This gives the asymptotic r dependence of the correlation function at large distances.

2. Interior of Hard Sphere

For $0<r<a$ we observe that the first and the second terms of Eq. (4.2) cancel by virtue of Eq. (4.3). Thus,

$$\begin{aligned}D^0(r)&=-\frac{1}{\rho\pi^3}\int\{1-q(q^2+\gamma_0)^{-1/2}-2^{-1}\gamma_0q^{-2}\}e^{2i\mathbf{q}\cdot\mathbf{r}}d\mathbf{q}\\ &=-(4a/r)\zeta\Phi(\zeta)+(2a/r).\end{aligned} \quad (4.11)$$

For small ζ Eq. (4.9) gives

$$\zeta\Phi(\zeta)=\tfrac{1}{2}-(4\zeta/3\pi)+O(\zeta^2). \quad (4.12)$$

Thus, we arrive at

$$D^0(r)=16a/3\pi r_c=O(a^3\rho)^{1/2}, \quad (4.13)$$

which is negligible in the low-density limit.

Summarizing, we find

$$\begin{aligned}D^0(r)&=1-16\pi^{1/2}(a^3\rho)^{1/2}\Phi(\zeta); \quad (r\gg a)\\ &=0; \quad (r<a).\end{aligned} \quad (4.14)$$

Since considerations have been confined to lowest-order diagrams, this result cannot be expected to apply in the immediate vicinity of the hard-sphere boundary. In a higher order calculation, using U_2 correct to second order in a, one expects

$$\begin{aligned}D^0(r)=&\left(1-\frac{a}{r}\right)^2-\frac{a}{r}\sum_{j=1}^\infty(-)^j\frac{(j+1)(j+2)}{[\Gamma(\frac{1}{2}j+2)]^2}\left(\frac{r}{2r_c}\right)^j\\ &+\text{contributions of next-to-lowest-order}\\ &\text{diagrams of 3 particles or more.}\end{aligned} \quad (4.15)$$

If one discards the last undetermined term, we have

$$\begin{aligned}D^0(r)&=\left(1-\frac{a}{r}\right)^2+\frac{16}{3\pi}\frac{a}{r_c}, \quad (a<r\ll r_c)\\ &=0(a^3\rho)^{1/2}, \quad (0<r<a).\end{aligned} \quad (4.16)$$

This coincides with the recent results of Luban (including the significant constant term related to the ground-state energy), who devised an accurate pseudopotential which accounts for the impenetrability of the spheres. Luban contrasts his findings with the LHY result which gives $D(r)$ for all $r\ll r_c$ including $r<a$.

V. THE CORRELATION FUNCTION $D^1(r)$

Using Eqs. (3.2), (3.3), (3.32), (3.33), and (3.34) we find

$$\begin{aligned}D^1(r)&=-\frac{2}{\pi^2r\rho}\int_0^\infty(\sum_m f_m{}^1)q\sin 2qrdq\\ &=-\frac{16}{\pi\rho\lambda^2r}\int_0^\infty\left\{\frac{1}{2\gamma}\frac{q^4}{(q^2+\gamma)^{3/2}}-\frac{q^3}{\gamma^2}\left(1-\frac{q}{(q^2+\gamma)^{1/2}}\right)\right.\\ &\qquad\left.+\frac{3}{8}\frac{q^2}{(q^2+\gamma)^{3/2}}\right\}\sin 2qrdq\\ &=\frac{1}{\rho\lambda^2r}\zeta\Theta(\zeta),\end{aligned} \quad (5.1)$$

where

$$\begin{aligned}\zeta\Theta(\zeta)\equiv&\left[\left(4\frac{\partial^2}{\partial\zeta^2}\frac{\partial}{\partial\alpha}-3\frac{\partial}{\partial\alpha}\right)(\alpha^3\zeta\Phi(a\zeta))\right]_{\alpha=1}\\ &-8\frac{\partial^2}{\partial\zeta^2}\zeta\Phi(\zeta).\end{aligned} \quad (5.2)$$

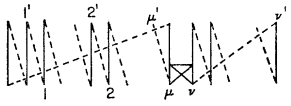

FIG. 4. Type-II, class A diagram.

The function $\zeta\Theta(\zeta)$ may be expressed in terms of I_ν and L_ν. Or, one can use the Hankel K function for $\zeta\Theta(\zeta)$. In any case, because of the recurrence formulas obeyed by these functions the right-hand side of Eq. (5.2) can be expressed in several different forms. However, since we have given $\zeta\Phi(\zeta)$ and its limiting forms in Eqs. (4.7), (4.9), (4.10), and (4.12), Eq. (5.2) is sufficient for our purposes. For small and large distances we find

$$\begin{aligned}\zeta\Theta(\zeta)&=-(4/5\pi)\zeta, \quad (\zeta\ll 1)\\ &=(12/\pi)\zeta^{-3} \quad (\zeta\gg 1).\end{aligned} \tag{5.3}$$

Thus, Eq. (5.1) gives

$$\begin{aligned}D^1(r)&=-\frac{1}{\rho\lambda^2}\frac{8\gamma_0^{1/2}}{5\pi}, \quad (a<r\ll r_c)\\ &=\frac{1}{\rho\lambda^2}\frac{3}{2\pi\gamma_0^{3/2}}\frac{1}{r^4} \quad (r\gg r_c).\end{aligned} \tag{5.4}$$

Combining $D^0(r)$ and $D^1(r)$ we end up with

$$D(r)=1-\frac{4a}{r}\zeta\Phi(\zeta)+\frac{1}{\rho\lambda^2 r}\zeta\Theta(\zeta),$$

where $\zeta=r/r_c$ and $r_c=(16\pi a\rho)^{-1/2}$ as defined by Eq. (4.5).

From these results we conclude that $D(r)$ decreases at short distances and increases at large distances as the temperature decreases. This means a larger long-distance correlation at lower temperature than has been discovered by recent x-ray and neutron experiments. Moreover, the dependence of $D(r)$ on temperature is not large and varies as $\lambda^{-2}\sim kT$.

VI. FIRST-ORDER BOSE DIAGRAMS

In this section we shall further investigate the p.d.f. for a finite temperature considering particle exchange in accordance with Bose statistics. Since our considerations are confined to first-order interactions, we are concerned with diagrams of the same type as treated by Colin and Peretti.[4] Our purpose in treating the same diagrams is mainly to correct the errors in their results. We therefore retain as much of the notation and approach of Colin and Peretti as suits our purpose best.

Free boson diagrams are called type I. Since their contribution to the p.d.f. is common knowledge, we begin with diagrams including the binary kernel. These

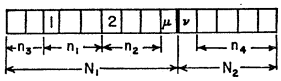

FIG. 5. Box diagram for type-II A diagrams.

are of two kinds: type II and type III. The former are characterized by two disjoint cycles of N_1 and N_2 particles coupled by a binary interaction; the latter consist of single cycles separated by the interacting pair into two parts consisting of N_1 and N_2 particles. Diagrams of the second and third kind are further subclassed as A and B according as the reference particles 1 and 2 appear on the same or opposite sides of the interacting pair.

1. Class A

We consider first diagrams of the second kind. Figure 4 shows the representative form and Fig. 5 is the "box diagram" which may be used to consider necessary combinatorial factors. Here the broad line between the particles μ and ν represents the interaction.

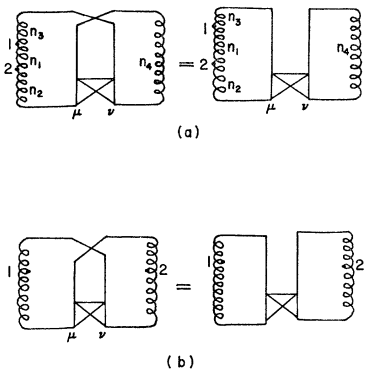

FIG. 6. (a) Type III A graph and its II A equivalent. (b) Type-III B graph and its II B equivalent.

For an l-particle diagram the integers n_i may take on values subject to

$$\begin{aligned}&N_1=n_1+n_2+n_3+1; && 1\leqslant n_1\leqslant N_1-1\\ &N_2=n_4+1; && 0\leqslant n_2\leqslant N_1-2\\ &2\leqslant N_1\leqslant l-1; && 0\leqslant n_3\leqslant N_1-2\\ &1\leqslant N_2\leqslant l-2; && 0\leqslant n_4\leqslant l-3\\ &N_1+N_2=l.\end{aligned} \tag{6.1}$$

As the n_i vary subject to these conditions, particles 1 and 2 march through the cells in Fig. 5 generating $\frac{1}{2}N_1(N_1-1)(l-2)!$ diagrams. The $(l-2)!$ corresponds to the permutations of the unnamed particles (including μ, ν).

The total number of diagrams of this type is given by

$$N_1(N_1-1)(l-2)!, \tag{6.2}$$

because a factor 2 should be introduced corresponding to the interchange of 1 and 2.

The momentum-space U function for these diagrams is

$$U_{n_i}{}^{\mathrm{II\,A}}(\mathbf{k}_1',\mathbf{k}_2';\mathbf{k}_1,\mathbf{k}_2)=-\frac{a}{\pi^2}\beta\left[\frac{\pi}{(n_1+1)\beta}\right]^{3/2}\delta(\mathbf{k}_1'-\mathbf{k}_2)$$
$$\times\delta(\mathbf{k}_2'-\mathbf{k}_1)\exp[-n_1\beta k_1^2-(n_2+n_3+1)\beta k_2^2]. \tag{6.3}$$

FIG. 7. Type-II B diagram. 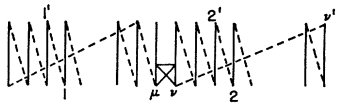

In coordinate space this gives

$$u_{n_i}^{\mathrm{IIA}}(r)=-(2a/\lambda^7)[n_1(n_2+n_3+1)(n_4+1)]^{-3/2}\times\exp\left[-\frac{r^2}{4\beta n_1}-\frac{r^2}{4\beta(n_2+n_3+1)}\right]. \quad (6.4)$$

The total contribution of type-II A l-particle diagrams is obtained by summing over all integers n_i subject to Eq. (6.1):

$$u_l^{\mathrm{IIA}}(r)=2(l-2)!\sum_{N_1}\sum_{N_2}\sum_{n_i}u_{n_i}^{\mathrm{IIA}}(r). \quad (6.5)$$

Since type-III A diagrams, of which a representative form appears in Fig. 6(a), give the same contribution to the p.d.f. as do type-II A, the contribution of class A diagrams of both kinds is

$$N_A(r)=2\sum_{l=3}^{\infty}\frac{z^l}{(l-2)!}u_l^{\mathrm{IIA}}(r)$$
$$=-\frac{8a}{\lambda^7}\sum_{n_4=1}^{\infty}\frac{z^{n_4}}{n_4^{3/2}}\sum_{n=1}^{\infty}\frac{z^n}{n^{1/2}}e^{-(s^2/n)}\sum_{n_1=1}^{\infty}\frac{z^{n_1}}{n_1^{3/2}}e^{-(s^2/n_1)},$$
$$=-(8a/\lambda^7)g_{3/2}(z)g_{1/2}(z,s)g_{3/2}(z,s), \quad (6.6)$$

where

$$g_\sigma(z,s)\equiv\sum_{n=1}\frac{z^n}{n^\sigma}e^{-(s^2/n)},$$
$$s^2\equiv r^2/4\beta=\pi r^2/\lambda^2, \quad (6.7)$$
$$g_\sigma(z)\equiv\sum_{n=1}^{\infty}(z^n/n^\sigma).$$

2. Class B

Diagrams wherein particles 1 and 2 are in separate cycles belong to type II B (Fig. 7). Correspondingly we have the box representation in Fig. 8. The n_i are restricted by

$$\begin{aligned}&N_1=n_1+n_2+1, \quad 0\leqslant n_1\leqslant N_1-1\\ &N_2=n_3+n_4+1, \quad 0\leqslant n_2\leqslant N_1-1\\ &1\leqslant N_1\leqslant l-1, \quad 0\leqslant n_3\leqslant N_2-1\\ &1\leqslant N_2\leqslant l-1, \quad 0\leqslant n_4\leqslant N_2-1\\ &N_1+N_2=l.\end{aligned} \quad (6.8)$$

The total number of type-II B graphs is

$$N_1N_2(l-2)!. \quad (6.9)$$

FIG. 8. Box representation for type-II B diagrams. 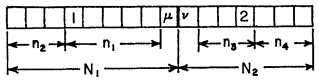

The evaluation of $u_l^B(r)$ is somewhat involved. In the initial stages the calculation proceeds in a manner identical with class A graphs. One finds

$$U_{n_i}^{\mathrm{IIB}}(\mathbf{k}_1',\mathbf{k}_2';\mathbf{k}_1,\mathbf{k}_2)$$
$$=-\frac{a}{\pi^2}\delta(\mathbf{k}_1'+\mathbf{k}_2'-\mathbf{k}_1-\mathbf{k}_2)\int_0^\beta d\beta_1$$
$$\times\exp\{-\beta[(n_2+1)k_1'^2+(n_4+1)k_2'^2+n_1k_1^2+n_3k_2^2]$$
$$+\beta_1[k_1'^2+k_2'^2-k_1^2-k_2^2]\}. \quad (6.10)$$

Unlike the case of class A graphs the coefficient of β_1 does not vanish. The β_1 integration itself is trivial but the resulting expression contains the factor $(k'^2-k^2)^{-1}$ which Colin and Peretti replaced by the principal part. We shall avoid this replacement by postponing the β_1 integration and Fourier inversion, and use the double momentum variable transformations of Eq. (3.6) to obtain $u_{n_i}(q)$. Summation on the n_i subject to Eq. (6.8) generates $u_l(q)$ from which $N^{\mathrm{IIB}}(q)$ follows via Eq. (3.2). Fourier inversion then gives $N_{\mathrm{IIB}}(r)$. Details of the calculation are given in Appendix B. We find

$$N_{\mathrm{IIB}}(r)=-\frac{a}{\lambda^6 r}\sum_{n_i=0}^{\infty}\{S(n_1+1,n_2,n_3+1,n_4;r)$$
$$-S(n_1,n_2+1,n_3,n_4+1;r)\}$$
$$=-\frac{2a}{\lambda^6 r}\sum_{n_1=1}^{\infty}\sum_{n_2=0}^{\infty}\sum_{n_3=1}^{\infty}\sum_{n_4=0}^{\infty}S(n_1,n_2,n_3,n_4;r). \quad (6.11)$$

Here

$$S(n_1,n_2,n_3,n_4;r)$$
$$=\frac{z^{n_1+n_2+n_3+n_4}}{(n_1+n_2)(n_3+n_4)(n_2+n_3)^{1/2}(n_1+n_4)^{1/2}}$$
$$\times\exp\left\{-\frac{n_1+n_2+n_3+n_4}{(n_2+n_3)(n_1+n_4)}\frac{r^2}{4\beta}\right\}\mathrm{erf}\{(n_1n_3-n_2n_4)r$$
$$\times(4\beta)^{-1/2}[(n_2+n_3)(n_1+n_4)$$
$$\times\{n_1n_3(n_2+n_4)+n_2n_4(n_1+n_3)\}]^{-1/2}\}. \quad (6.12)$$

Class B diagrams of the third kind contribute the same amount. [See Fig. 6(b).] Thus altogether

$$N_B(r)=-\frac{4a}{\lambda^6 r}\left\{\sum_{n_1=1}^{\infty}\sum_{n_3=1}^{\infty}\frac{z^{n_1+n_3}}{(n_1n_3)^{3/2}}\exp\left[-\left(\frac{1}{n_1}+\frac{1}{n_3}\right)\frac{r^2}{4\beta}\right]\right.$$
$$+2\sum_{l=1}^{\infty}\sum_{m=1}^{\infty}\sum_{n=1}^{\infty}\frac{z^{l+m+n}}{(l+m)nl^{1/2}(m+n)^{1/2}}$$
$$\times\exp\left\{-\frac{l+m+n}{l(m+n)}\frac{r^2}{4\beta}\right\}$$
$$\left.\times\mathrm{erf}[nr(4\beta(m+n)mn)^{-1/2}]\right\}. \quad (6.13)$$

Here the first term corresponds to the case $n_2=n_4=0$ for which the error function is unity. The second term

arises from

$$\sum_{n_1=1}^{\infty}\sum_{n_3=1}^{\infty}\sum_{n_4=1}^{\infty} S(n_1,0,n_3,n_4;r) = \sum_{n_1=1}^{\infty}\sum_{n_2=1}^{\infty}\sum_{n_3=1}^{\infty} S(n_1,n_2,n_3,0;r). \quad (6.14)$$

The remaining sum

$$\sum_{n_1,\,n_2,\,n_3,\,n_4=1}^{\infty} S(n_1,n_2,n_3,n_4;r)$$

vanishes as a consequence of the antisymmetry of S upon exchange of the pair (n_1,n_3) with (n_2,n_4).

We are now in a position to summarize the first-order results. From Eqs. (6.6) and (6.13), one obtains

$$D(r)=1+\left[\frac{1}{\rho\lambda^3}g_{3/2}(z,s)\right]^2-\frac{8a}{\rho^2\lambda^7}g_{3/2}(z)g_{1/2}(z;s)g_{3/2}(z;s) -\frac{4a}{r}\left[\frac{1}{\rho\lambda^3}g_{3/2}(z;s)\right]^2-\frac{8a}{\rho^2\lambda^7}\frac{\lambda}{r} \times\sum_{l,m,n=1}^{\infty}\frac{z^{l+m+n}}{(l+m)nl^{1/2}(m+n)^{1/2}}\exp\left\{-\frac{l+m+n}{l(m+n)}s^2\right\} \times\operatorname{erf}(ns((m+n)mn)^{-1/2}), \quad (6.15)$$

where the second term represents the noninteracting case.

In the remainder of this section we shall evaluate the singlet distribution function because it is necessary to find z as a function of ρ and λ.

Three kinds of diagrams occur as in the case of the p.d.f. Diagrams of the first kind, corresponding to free particles, are easy to treat. One finds

$$\sum_{l=1}^{\infty}\frac{z^l}{(l-1)!}u_l^{\mathrm{I}}(\mathbf{r}_1)=\frac{1}{\lambda^3}g_{3/2}(z). \quad (6.16)$$

Diagrams of the second kind contribute

$$u_l^{\mathrm{II}}(\mathbf{r}_1)=-\frac{2a}{\lambda^4}(l-1)!\sum_{N_1,N_2=1}^{l-1\;\;l-1}N_1(N_1N_2)^{-3/2}, \quad N_1+N_2=l. \quad (6.17)$$

The factor N_1 is due to the N_1 positions available to the reference particle, and $(l-1)!$ corresponds to the permutations of the remaining particles. Thus, adding the equal contributions from diagrams of the third kind and summing on l we have

$$2\sum_{l=1}^{\infty}\frac{z^l}{(l-1)!}u_l^{\mathrm{II}}(\mathbf{r}_1)=-\frac{4a}{\lambda^4}\sum_{l=2}^{\infty}z^l\sum_{N_1,N_2=1}^{l-1\;\;l-1}N_1^{-1/2}N_2^{-3/2} =(-4a/\lambda^4)g_{1/2}(z)g_{3/2}(z). \quad (6.18)$$

Combining Eqs. (6.16) and (6.18) we end up with

$$\rho^{(1)}=(1/\lambda^3)g_{3/2}(z)-(4a/\lambda^4)g_{1/2}(z)g_{3/2}(z). \quad (6.19)$$

This is exactly what one can obtain from Lee and Yang's grand partition function.

VII. CONCLUDING REMARKS

The p.d.f. obtained in the previous section differs from that reported by Colin and Peretti.[4] (In comparing results we note that our "a" represents the hard-sphere diameter, whereas the "a" appearing in their Eq. (47) is the radius.) First, in summing class A diagrams, it appears they have overlooked a factor of 2 associated with an interchange of particles 1 and 2. Second, the contribution of class B diagrams is different. In this respect, their result corresponds to neglect of the last term in Eq. (6.15).

The correctness of our result may be demonstrated by checking the normalization. We easily find

$$\begin{aligned}\int\int[\rho^{(2)}(r)-\rho^2]d\mathbf{r}_1d\mathbf{r}_2 &=(V/\lambda^3)\{g_{1/2}(z)-g_{3/2}(z)-(4a/\lambda)g_{3/2}(z)\\ &\quad\times(g_{-1/2}(z)-g_{1/2}(z))-(4a/\lambda)g_{1/2}{}^2(z)\},\\ &=(\partial\langle N\rangle/\partial\log z)-\langle N\rangle, \end{aligned} \quad (7.1)$$

where the last equality is obtained by using the singlet distribution function given by Eq. (6.19).

At this point we may call attention to a result obtained by Bogoliubov's formalism in Colin's second paper.[10]

$$D(r)-1=[(1/\rho\lambda^3)g_{3/2}(z;s)]^2-(8a/\rho^2\lambda^7) \times g_{3/2}(z)g_{1/2}(z;s)g_{3/2}(z;s). \quad (7.2)$$

Here we have used a for the hard-sphere diameter. This coincides with the first three terms of Eq. (6.15). Colin[10] noticed the discrepancy between this expression and the corresponding one in Colin and Peretti's binary-kernel approach but argued that the difference was inherent in the methods.

Returning to our results based on Boltzmann chain diagrams we comment that Lieb[11] obtained results similar to ours. In the process of evaluating the ground-state energy he defined *certain distribution functions* $g^{(n)}(r_1,\cdots,r_n)$ in terms of the wave function itself rather than its square. His results are therefore fundamentally different from ours but the similarity is interesting. He obtained

$$\begin{aligned} g(r)&=1-32\pi^{1/2}(a^3\rho)^{1/2}U(R); \quad (r>a)\\ &=0; \quad (r<a), \end{aligned} \quad (7.3)$$

where

$$\begin{aligned} R&\sim 4(\pi a\rho)^{1/2}r,\\ U(R)&=(1/R^3)\{R[I_1(R)-L_1(R)] -3[I_2(R)-L_2(R)]\}. \end{aligned} \quad (7.4)$$

[10] L. Colin, J. Math. Phys. **1**, 87 (1960).
[11] E. H. Lieb, Phys. Rev. **130**, 2518 (1963).

Using our notation

$$R=r/r_c=\zeta.$$

Equation (7.3) resembles Eq. (4.14).

The limiting forms of $U(R)$ give

$$g(r)=1-\frac{a}{r}+\frac{128}{15}\left(\frac{a^3\rho}{\pi}\right)^{1/2}; \quad (a<r\ll r_c)$$

$$=1-128\left(\frac{a^3\rho}{\pi}\right)^{1/2}\left(\frac{r_c}{r}\right)^4; \quad (r\gg r_c). \tag{7.5}$$

For large distances Lieb's $g(r)-1$ is greater than our $D^0(r)-1$ by a factor of 2. At short distances one may compare the expression in Eq. (7.5) with Eq. (4.16) which is expected from a higher order calculation.

Lowest order diagrams do not give a physically acceptable p.d.f. in the vicinity of $r=a$. This is because the short-range behavior of the p.d.f. is essentially determined by the two-particle cluster function of Eq. (4.3) which is discontinuous at $r=a$ when taken to first order in a. Continuity is recovered with the second-order term and $\rho^{(2)}(r)\to 0$ as $r\to a$. This clearly points to the desirability of a higher order calculation.

APPENDIX A: EVALUATION OF THE FOURIER TRANSFORM

We write

$$(1-\eta(\eta^2+1)^{-1/2})\eta=(\eta^2+1)^{-1/2}-\{(\eta^2+1)^{1/2}+\eta\}^{-1/2}, \tag{A1}$$

and note

$$\frac{1}{(\eta^2+1)^{1/2}}=\int_0^\infty J_0(t)e^{-\eta t}dt,$$
$$\frac{1}{(\eta^2+1)^{1/2}+\eta}=\int_0^\infty \frac{J_1(t)}{t}e^{-\eta t}dt. \tag{A2}$$

Thus

$$\int_0^\infty\left\{1-\frac{\eta}{(\eta^2+1)^{1/2}}\right\}\eta\sin\eta\zeta d\eta=\zeta\int_0^\infty\left\{\frac{J_0(t)}{t^2+\zeta^2}-\frac{J_1(t)}{t(t^2+\zeta^2)}\right\}dt. \tag{A3}$$

We can make use of the formula for Hankel–Nicholson-type integrals:

$$\int_0^\infty\frac{J_\nu(at)}{t^\nu(t^2+z^2)}dt=\frac{\pi}{2z^{\nu+1}}[I_\nu(az)-L_\nu(az)]$$
$$=(\pi/2z^{\nu+1})G_\nu(az). \tag{A4}$$

Thus we arrive at

$$\int_0^\infty\left\{1-\frac{\eta}{(\eta^2+1)^{1/2}}\right\}\eta\sin\eta\zeta d\eta=\frac{\pi}{2}\left[G_0(\zeta)-\frac{1}{\zeta}G_1(\zeta)\right]. \tag{A5}$$

APPENDIX B: INTEGRALS ASSOCIATED WITH TYPE-B DIAGRAMS

We are concerned with the integral appearing in

$$N^{\mathrm{IIB}}(q)=-\frac{64\pi a}{\beta^{3/2}}\sum_{n_i=0}^{\infty}\frac{z^l}{l^{3/2}D^3}e^{-\alpha q^2}\int_0^\beta d\beta_1 e^{\xi^2q^2}, \tag{B1}$$

where

$$\begin{aligned}\alpha&=(4\beta/l)(n_2+n_3+1)(n_1+n_4+1);\\ D\xi&=(4\beta/l)[(n_2+1)(n_4+1)-n_1n_3]-4\beta_1;\\ D^2&=(4\beta/l)(n_1+n_2+1)(n_3+n_4+1);\\ l&=n_1+n_2+n_3+n_4+2.\end{aligned} \tag{B2}$$

We note

$$\int_0^\beta e^{\xi^2(\beta_1)q^2}d\beta_1=\frac{\pi^{1/2}D}{8q}\left\{\mathrm{erfi}\left(\left(\frac{4\beta}{l}\right)^{1/2}q\frac{(n_1+1)(n_3+1)-n_2n_4}{(n_1+n_2+1)^{1/2}(n_3+n_4+1)^{1/2}}\right)-\mathrm{erfi}\left(\left(\frac{4\beta}{l}\right)^{1/2}q\frac{n_1n_3-(n_2+1)(n_4+1)}{(n_1+n_2+1)^{1/2}(n_3+n_4+1)^{1/2}}\right)\right\}, \tag{B3}$$

where

$$\mathrm{erfi}(x)=\frac{2}{\pi^{1/2}}\int_0^x e^{t^2}dt. \tag{B4}$$

We define

$$\Omega(n_1,n_2,n_3,n_4;q)=\frac{z^{n_1+n_2+n_3+n_4}}{(n_1+n_2+n_3+n_4)^{1/2}(n_1+n_2)(n_3+n_4)}\times\frac{1}{q}\exp\left\{-\frac{(n_2+n_3)(n_1+n_4)}{n_1+n_2+n_3+n_4}4\beta q^2\right\}\times\mathrm{erfi}\left\{\frac{(n_1n_3-n_2n_4)(4\beta)^{1/2}q}{(n_1+n_2)^{1/2}(n_3+n_4)^{1/2}(n_1+n_2+n_3+n_4)^{1/2}}\right\} \tag{B5}$$

and note

$$\Omega(\alpha,\beta,\gamma,\delta;q)=-\Omega(\beta,\alpha,\delta,\gamma;q). \tag{B6}$$

Thus,

$$N^{\mathrm{IIB}}(q)=-\frac{4\pi^{3/2}a}{\beta^{5/2}}\sum_{n_1=1}\sum_{n_2=0}\sum_{n_3=1}\sum_{n_4=0}\Omega(n_1,n_2,n_3,n_4;q). \tag{B7}$$

The Fourier inversion of $\Omega(n_i;q)$ is

$$\int\Omega(n_i;q)e^{2i\mathbf{q}\cdot\mathbf{r}}d\mathbf{q}=\frac{\pi^{3/2}}{(4\beta)^{1/2}r}S(n_i;r), \tag{B8}$$

where $S(n_i;r)$ is defined in Eq. (6.12). Then Eq. (6.11) follows from

$$N_{\mathrm{IIB}}(r)=\frac{1}{(2\pi)^6}\int N^{\mathrm{IIB}}(q)e^{2i\mathbf{q}\cdot\mathbf{r}}d\mathbf{q}. \tag{B9}$$